CHEMISTRY
A EUROPEAN JOURNAL

DOI: 10.1002/chem.200701348

Spontaneous Organization of Uniform CeO_2 Nanoflowers by 3D Oriented Attachment in Hot Surfactant Solutions Monitored with an In Situ Electrical Conductance Technique

Huan-Ping Zhou,[a] Ya-Wen Zhang,*[a] Hao-Xin Mai,[a] Xiao Sun,[a] Qiang Liu,[b] Wei-Guo Song,[b] and Chun-Hua Yan*[a]

Abstract: Uniform CeO_2 nanoflowers were synthesized by rapid thermolysis of $(NH_4)_2Ce(NO_3)_6$ in oleic acid (OA)/oleylamine (OM), by a unique 3D oriented-attachment mechanism. CeO_2 nanoflowers with controlled shape (cubic, four-petaled, and starlike) and tunable size (10–40 nm) were obtained by adjusting the reaction conditions including solvent composition, precursor concentration, reaction temperature, and reaction time. The nanoflower growth mechanism was investigated by in situ electrical conductance measurements, transmission electron microscopy, and UV/Vis spectroscopy. The CeO_2 nanoflowers are likely formed in two major steps, that is, initial formation of ceria cluster particles capped with various ligands (e.g., OA, OM, and NO_3^-) via hydrolysis of $(NH_4)_2Ce(NO_3)_6$ at temperatures in the range 140–220 °C, and subsequent spontaneous organization of the primary particles into nanoflowers by 3D oriented attachment, due to a rapid decrease in surface ligand coverage caused by sudden decomposition of the precursor at temperatures above 220 °C in a strong redox reaction. After calcination at 400 °C for 4 h the 33.8 nm CeO_2 nanoflowers have a specific surface area as large as 156 $m^2 g^{-1}$ with high porosity, and they are highly active for conversion of CO to CO_2 in the low temperature range of 200–400 °C. The present approach has also been extended to the preparation of other transition metal oxide (CoO, NiO, and CuO_x) nanoflowers.

Keywords: ceria · cerium · crystal growth · nanostructures · self-assembly

Introduction

Colloidal inorganic nanocrystals with controlled dimensionality (e.g., 0D dots,[1a–d] 1D rods[1e,f] and wires,[1g] 2D plates[1h,i] and disks,[1i,j] and 3D flowers[1k,l]) are versatile building blocks for constructing diverse superstructures, functional mesocrystals, and new nanodevices, which are scientifically important and technologically useful in multidisciplinary fields of chemistry, physics, materials science, nanoscience, nanotechnology, biology, and medicine.[1–4] More recently, nanocrystal assemblies with advanced 3D architectures of metal oxides (e.g., CoO, MnO, ZnO, and In_2O_3),[1k,l] II–VI semiconducting compounds (e.g., ZnSe[1k] and CdSe[2a]), and metals (e.g., Co,[2b] Au,[2c,d] and PtRu[2e]) have attracted particular interest because of their potential in solar cells, magnets, catalysts, and optical materials. More importantly, a 3D nanostructure is composed of small-sized building blocks hierarchically, while the total size approaches the submicrometer and micrometer scales. Because such superstructures combine microstructure and nanostructure, they may exhibit new material properties.[2]

[a] H.-P. Zhou, Prof. Dr. Y.-W. Zhang, H.-X. Mai, Dr. X. Sun, Prof. Dr. C.-H. Yan
Beijing National Laboratory for Molecular Sciences
State Key Laboratory of Rare Earth Materials Chemistry and Applications
PKU-HKU Joint Laboratory in Rare Earth Materials and Bioinorganic Chemistry
Peking University, Beijing 100871 (China)
Fax: (+86) 10-6275-4179
E-mail: yan@pku.edu.cn
ywzhang@pku.edu.cn

[b] Q. Liu, Prof. Dr. W.-G. Song
Institute of Chemistry, Chinese Academy of Sciences
Beijing 100080 (China)

Supporting information for this article is available on the WWW under http://www.chemeurj.org/ or from the author. It includes TEM and HRTEM images of CeO_2 nanocrystals; plots of the variation of electrical resistance with reaction temperature and time; TG-DTA curve of $(NH_4)_2Ce(NO_3)_6$; UV/Vis and IR spectra of some Ce-containing species and solvents; TEM image and N_2 adsorption/desorption isotherm of as-calcined CeO_2 nanoflowers; XRD patterns, TEM images, and XPS survey spectra of CoO, NiO, and CuO_x nanocrystals; and magnetization versus absolute temperature curve of CoO nanoflowers under an applied field of 1000 Oe.

The development of robust synthetic methodologies is the most important means of manipulating the dimensionality and material properties of the nanobuilding blocks and their 3D structured assemblies.[1–3] So far, the nonhydrolytic approach, in which the nucleation and growth stages are performed apart, offers convenience in preparing high-quality nanocrystals and complex 3D structures derived therefrom.[1–3,5] A comprehensive understanding of nanocrystal growth kinetics in this approach is crucially important, not only for reproducible large-scale fabrication of high-quality products with manipulated nanostructures, but also for correct interpretation of the collective material properties of an ensemble of particles in terms of the features of an individual particle. Besides in situ UV/Vis spectroscopy, the introduction of other effective in situ detection techniques to nanocrystal syntheses in solutions can lead to improved control of nanocrystal growth regimes (kinetic or thermodynamic) to obtain designed nanostructures.[5]

Recently, much attention has been paid to shape-/size-controlled dispersible nanostructures of metal oxide (e.g., rare earths[1i] and transition metal oxides[1d,g,k,l]) with unique material properties, which have theoretical and technological significance.[6,7] Ceria (CeO_2) is widely used in conversion catalysts[6a,b] three-way catalysts,[6c,d] fuel cells,[6e] solar cells,[6f] gates for metal-oxide semiconductor devices,[6g] and phosphors.[6h] In addition, transition metal oxide nanocrystals[1d,g,k,l,5a] are of increasing importance in technical applications such as magnetic data storage, magnetic resonance imaging, drug delivery, energy storage, catalysts, biosensing, sensors, and ferrofluids.[7] To date, there have been few reports on the synthesis of dispersible 3D structures of metal oxides.[1k,l,2] Recently, Peng et al. obtained colloidal crystalline nanoflowers of metal oxides (CoO, MnO, ZnO, and In_2O_3) by a general solution methodology involving the limited ligand protection (LLP) mechanism.[1k,l] However, it still remains a challenge to develop a new general route for the synthesis of well-controlled 3D structures of CeO_2 and other metal oxides.

Here we report the controllable synthesis of uniform CeO_2 nanoflowers by rapid thermolysis of $(NH_4)_2Ce(NO_3)_6$ in oleic acid (OA)/oleylamine (OM). CeO_2 nanoflowers with controllable shape (cubic, four-petaled, and starlike) and size (10–40 nm) were obtained by adjusting the reaction parameters (e.g., solvent composition, precursor concentration, reaction temperature, and reaction time). For the first time, an in situ electrical conductance technique has been employed to monitor the growth kinetics of the nanoflowers in solution. With the further assistance of transmission electron microscopy (TEM) and UV/Vis spectroscopy, formation of nanoflowers has been demonstrated to proceed by a unique 3D oriented-attachment mechanism. By the same approach, some other transition metal oxide (CoO, NiO, and CuO_x) nanoflowers have also been prepared. Moreover, the as-prepared CeO_2 and CoO nanoflowers show interesting material properties.

Abstract in Chinese:

采用硝酸铈铵在油酸和油胺混合溶剂中的快速热分解反应，合成了尺寸(10 – 40 nm)和形貌(方形、四花瓣形或星形)可控的“花状” CeO_2 纳米晶。提出了以简单的原位电导测量方法监测纳米晶生成过程的技术，进而结合 TEM、UV-vis 光谱等表征技术，对纳米花的生成机理进行了讨论：当体系温度低于 220 °C 时，硝酸铈铵经水解生成 1 – 2 nm 的 CeO_2 颗粒，这些小颗粒被油酸、油胺和硝酸根离子等配体络合包覆；当体系温度升高至 220 °C 以上，强烈的氧化还原反应使 CeO_2 颗粒表面的配体急剧缺失，导致小颗粒通过3-D取向连接、自发组织成 CeO_2 纳米花。研究表明，CeO_2 纳米花经 400 °C 烧结 4 h 后仍具较大的比表面积 (156 m^2g^{-1})，且在 200 – 400 °C 温区对 CO 的氧化呈现良好的催化活性。该方法还可用于过渡金属氧化物(CoO、NiO 和 CuO_x)纳米花的合成。

Results and Discussion

Structure, size, shape, oxidation state, and band-gap energy of CeO_2 nanoflowers: In the X-ray diffraction (XRD) patterns of as-obtained CeO_2 nanoflowers of different sizes (Figure 1a), five intense, well-resolved peaks in the range of $2\theta = 25–65°$ are respectively ascribed to (111), (200), (220), (311), and (222) crystal planes of a cubic fluorite structure (space group: $Fm\bar{3}m$). The moderate broadening of the reflections suggests relatively large size of the nanoflowers. The calculated lattice constants of 37.6, 33.8, and 19.7 nm (TEM size) CeO_2 nanoflowers of $a = 5.427(2)$, 5.398(4), and 5.428(3) Å, respectively, coincide with the theoretical value of 5.411 Å for bulk CeO_2 (JCPDS: 34-394). The calculated XRD crystal domain sizes for the three nanoflowers samples are 14.5, 11.4, and 10.03 nm, respectively.

Figure 1 b–f show TEM and HRTEM images of the as-obtained CeO_2 nanoflowers. The nanoflowers made of small ceria nanoparticles organized by orientated attachment are cube-shaped (see Figure 1b,e,f) and form partially ordered arrays on the copper grids due to their size uniformity and effective surface passivation by the capping ligands (mainly oleic acid) with hydrophobic long alkyl chains (see FTIR results in Figure S1 in the Supporting Information). The sizes of the nanoflowers were determined to be (33.8 ± 2.3) (Figure 1b), (37.6 ± 2.6) (Figure 1e), and (19.7 ± 1.5) nm (Figure 1f). The fact that the calculated XRD domain size is significantly smaller than the TEM size demonstrates that the ceria nanoflowers are aggregates of small ceria nanoparticles.[8] Figure 1c shows an HRTEM image of a single 33.8 nm CeO_2 nanoflower. The clearly visible lattice fringes are indicative of the high crystallinity of the nanoflower. The interplanar distance of 0.27 nm can be indexed to the (200) or (020) plane of cubic CeO_2, while the interplanar distance of 0.19 nm is ascribed to the (220) plane. The CeO_2 nanoflower mainly exposes {100} planes, with rather rough surface but no appreciable amorphous phase. Moreover, some small ceria crystallites (cluster particles) are anchored on the surface of the CeO_2 nanoflower, oriented along a direction that intersects with the {100} planes at an angle of

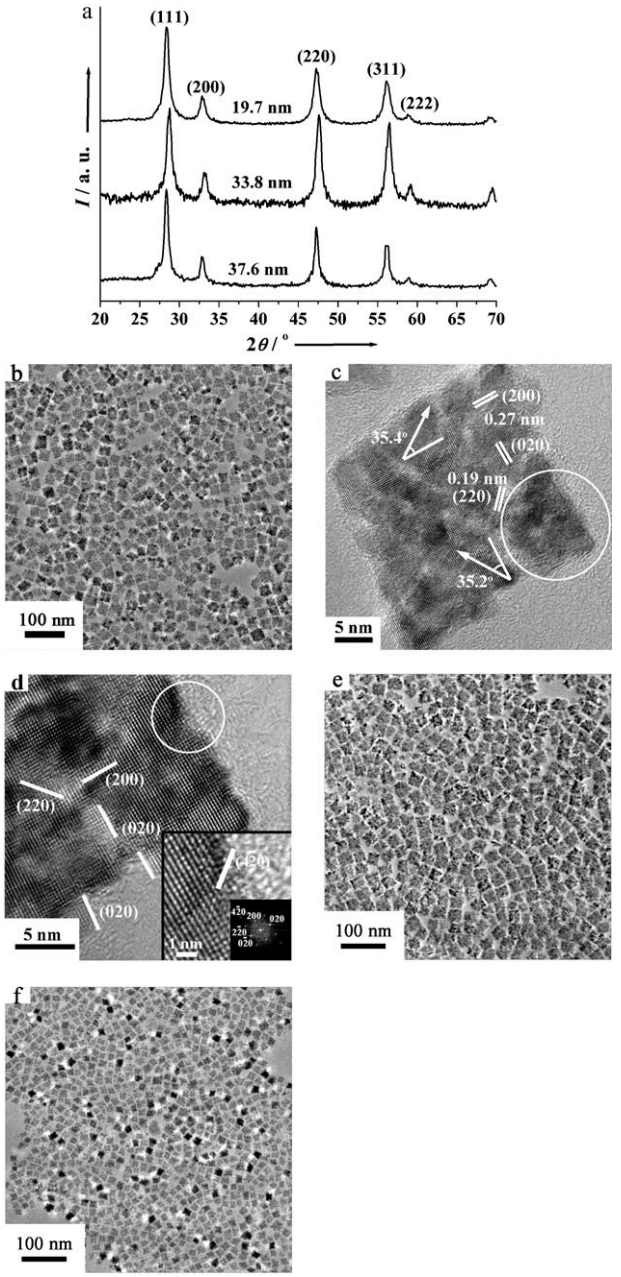

Figure 1. a) XRD patterns of CeO_2 nanoflowers. b) TEM image of 33.8 nm CeO_2 nanoflowers. c) HRTEM image of a single 33.8 nm CeO_2 nanoflower. d) HRTEM image of a corner (as taken from the highlighted circle in c) of a single 33.8 nm CeO_2 nanoflower at high magnification; the inset shows the HRTEM image and FFT pattern of an edge area around the corner (as taken from the upper highlighted circle) of the nanoflower at high magnification. TEM images of e) 37.6 nm and f) 19.7 nm CeO_2 nanoflowers.

about 35°, which suggests that the direction of oriented attachment is along [111] (see below). Perhaps because the CeO_2 nanoflowers are formed by oriented aggregation of ceria clusters, many defective interfaces such as dislocations and distortions are observable in their HRTEM images. The HRTEM image of the highlighted corner of a single nanoflower (Figure 1d) indicates that the defective interfaces are mainly {100} planes, along with some {110} planes. Furthermore, some high-index planes (e.g., (420) planes) are observed in the defective interfaces (see inset in Figure 1d). According to the literature,[9] the (200) plane and especially the (420) plane have relatively high surface energy among the high-index planes.

Figure 2a and b show a typical XPS survey spectrum of the as-obtained CeO_2 nanoflowers and the corresponding XPS signal of the Ce 3d core levels, respectively. In Figure 2a, peaks attributed to the core levels of Ce 3d, Ce 4d, O 1s, C 1s, and N 1s can be identified for the surfactant-capped CeO_2 nanoflowers. For the Ce 3d core levels, the appearance of an intense binding energy (BE) peak at 916.6 eV, along with five other strong peaks at 882.2, 888.8, 898.1, 900.8, and 907.5 eV, strongly suggests that the oxidation state of cerium in the nanoflowers is predominantly tetravalent.[10] Figure 3a shows a representative Raman spectrum of the CeO_2 nanoflowers. Only one intense Raman peak originating from the Raman-active F_{2g} mode (a symmetrical stretching mode of the Ce–8O vibrational unit) of cubic CeO_2 is observed at 462 cm^{-1}, which agrees with the Raman shift value of CeO_2 nanocrystalline films[11a] and single crystal.[11b] Since this Raman peak is only slightly asymmetric and a little broadened, disorder in the oxygen sublattice of the nanoflowers is low.[11]

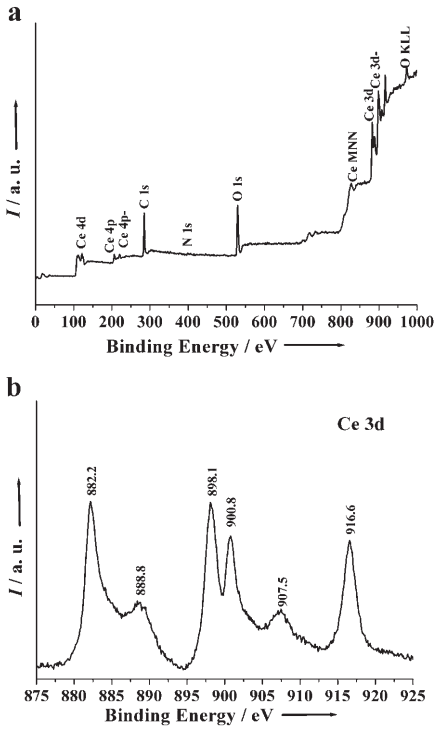

Figure 2. XPS patterns of CeO_2 nanoflowers: a) survey spectra and b) Ce 3d core levels.

Figure 3b shows the UV/Vis absorption spectra of the as-obtained CeO_2 nanoflowers dispersed in hexanes. The strong absorption band with an edge below 400 nm is due to

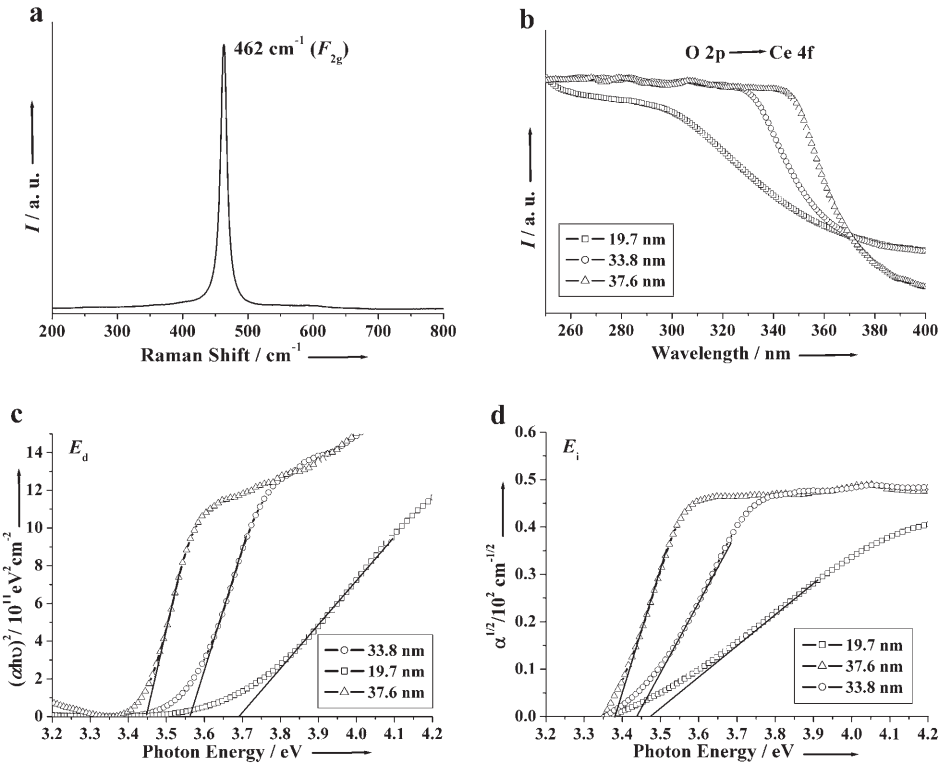

Figure 3. a) Raman spectrum of 33.8 nm CeO_2 nanoflowers. Electronic band-gap measurement of differently sized CeO_2 nanoflowers: b) UV/Vis absorption spectra; c) plot of $(\alpha h\nu)^2$ versus photon energy; d) plot of $\alpha^{1/2}$ versus photon energy.

charge-transfer transitions from O 2p to Ce 4f,[12] rather than absorption by the capping ligands (see Figure S2 in the Supporting Information). Interestingly, the UV absorption-edge wavelength shows a blue shift from about 348 nm for 37.6 nm nanoflowers to about 332 nm for 33.8 nm nanoflowers, and to about 307 nm for 19.7 nm nanoflowers. The optical band gap E_g of a semiconductor material can be calculated from the equation of $(\alpha h\nu)^n = B(h\nu - E_g)$, where $h\nu$ is the photon energy, α the absorption coefficient, B a constant for the material, and n is 2 for a direct transition or 1/2 for an indirect transition.[12] As the size of nanoflowers decreases from 37.6 to 33.8 and then to 19.7 nm, the calculated direct band-gap energy E_d increases from 3.45 to 3.56 and then to 3.69 eV (see Figure 2c), which is comparable to the value of 3.6 eV for CeO_2 single crystal and polycrystalline films,[12a,b] and the calculated indirect band-gap energy E_i increases from 3.38 to 3.44 and then to 3.47 eV, all of which are greater than that of 3.2 eV for CeO_2 single crystal and polycrystalline films.[12a,b] Considering the quite large size (significantly greater than 10 nm) of our CeO_2 nanoflowers, we propose that the UV blue shift with decreasing size of the nanoflowers does not arise from confinement effects.[12c–f] Moreover, since the valence of cerium in our flowers is +4 (as revealed by XPS), this blue shift should also not be attributed to the Ce^{III}-related effects observed by some groups.[12d] As demonstrated before, the presence of surface defects can cause the UV absorption edge of ceria to shift to longer wavelength (red shift).[12e,f] We found that the smaller the nanoflowers, the better the passivation of surface defects by the capping ligands (see FTIR results in Figure S1 in the Supporting Information). Therefore, the blue shift in band-gap energy predominates for the differently sized nanoflowers in the present case.

Formation conditions of CeO_2 nanoflowers: The controlled synthesis of monodisperse 3D nano-objects with complex structures and compositions is extensively studied nowadays, but have been insufficiently investigated for colloidal inorganic nanoparticles.[1k,l,2] Formation of the CeO_2 nanoflowers is highly dependent on several synthetic parameters, such as type of precursor, surfactant molar ratio (oleic acid to oleylamine), precursor concentration, reaction temperature, and reaction time.

Type of precursor: $(NH_4)_2Ce(NO_3)_6$ plays a unique role as precursor in the present synthesis of CeO_2 nanoflowers, and is not replaceable by other cerium compounds such as $Ce(NO_3)_3{\cdot}6H_2O$ and $Ce(OH)_4$. For example, when 1 mmol of $Ce(NO_3)_3{\cdot}6H_2O$ was used as precursor, reaction at 300 °C for 1 h with OA:OM = 1:3 produced a mixture of polydisperse CeO_2 nanocrystals and randomly aggregated assemblies thereof (Figure 4a). The use of 1 mmol of $Ce(OH)_4$ as precursor yielded aggregates of ultrafine CeO_2 nanocrystals (Figure 4b). Moreover, we found that no CeO_2 nanoflowers but only gels or low-crystallinity nanoparticles were formed on using both NH_4NO_3 and $Ce(OH)_4$ (or $Ce(NO_3)_3{\cdot}6H_2O$) as precursors. However, when $Ce(NO_3)_3{\cdot}6H_2O$ and $Ce(OH)_4$ were replaced by $(NH_4)_2Ce(NO_3)_6$, 33.8 nm CeO_2

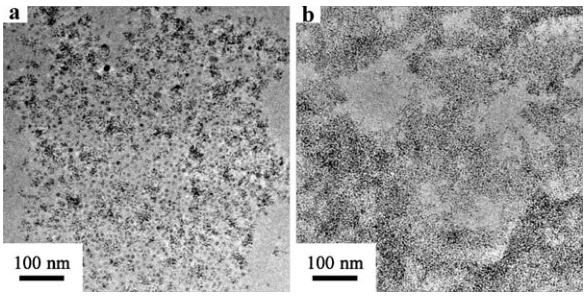

Figure 4. TEM images of CeO_2 nanocrystals synthesized at 300 °C for 1 h with OA:OM = 1:3 and 1 mmol of a) $Ce(NO_3)_3{\cdot}6H_2O$ and b) $Ce(OH)_4$ as precursor.

Table 1. Crystal structure, morphology, and size of MO_x (M = Ce, Co, Ni, Cu) nanocrystals synthesized in 40 mmol of OA:OM.

	Precursor	OA:OM	T [°C]	t [min]	Structure	Morphology	Size[a] [nm]
CeO_2	1 mmol $(NH_4)_2Ce(NO_3)_6$	1:3	300	240	cubic	cube-shaped flower	37.6 ± 2.6
CeO_2	1 mmol $(NH_4)_2Ce(NO_3)_6$	1:3	300	60	cubic	cube-shaped flower	33.8 ± 2.3
CeO_2	1 mmol $(NH_4)_2Ce(NO_3)_6$	2:3	280	15	cubic	cube-shaped flower	19.7 ± 1.5
CeO_2	1 mmol $(NH_4)_2Ce(NO_3)_6$	0	300	60	cubic	polyhedra	4.3 ± 0.7
CeO_2	1 mmol $(NH_4)_2Ce(NO_3)_6$	1:20	300	60	cubic	polyhedra	4.5 ± 0.5
CeO_2	1 mmol $(NH_4)_2Ce(NO_3)_6$	1:6	300	60	cubic	polyhedra	4.8 ± 0.8
CeO_2	0.5 mmol $(NH_4)_2Ce(NO_3)_6$	1:3	300	60	cubic	cube-shaped flower	17.8 ± 1.1
CeO_2	0.2 mmol $(NH_4)_2Ce(NO_3)_6$	1:3	300	60	cubic	cube-shaped flower	16.3 ± 2.4
CeO_2	1 mmol $(NH_4)_2Ce(NO_3)_6$	1:3	230	30	cubic	four-petaled flower	28.5 ± 1.9
CeO_2	1 mmol $(NH_4)_2Ce(NO_3)_6$	2:3	300	60	cubic	star-shaped flower	10.6 ± 1.4
CoO	0.4 mmol $(NH_4)_3Co(NO_3)_5$	1:2	240	30	cubic	flower	74.6 ± 13.0
NiO	0.4 mmol $(NH_4)_3Ni(NO_3)_5$	1:6	240	30	cubic	flower	10.4 ± 0.85
CuO_x	0.4 mmol $(NH_4)_3Cu(NO_3)_5$	0:1	280	5	cubic	flower	27.5 ± 2.73

[a] Standard deviations for 100 nanocrystals.

nanoflowers were obtained under the same conditions (Figure 1b and Table 1).

Ratio of OA to OM: The morphology of the CeO_2 nanocrystals can be tuned by changing the ratio of OA to OM ($R_{OA/OM}$). When $R_{OA/OM}$ was less than 1:6, (4.3 ± 0.7) and (4.5 ± 0.5) nm CeO_2 nanopolyhedra were obtained at 300 °C for 1 h with 1 mmol of $(NH_4)_2Ce(NO_3)_6$ as precursor (Figure 5a and Figure S3a in the Supporting Information, and Table 1). With increasing amount of OA, strongly agglomerated polydisperse CeO_2 nanocrystals of relatively large size (4.8 ± 0.8) were formed (Figure 5b and Table 1) at $R_{OA:OM}$ = 1:6, whereas (33.8 ± 2.3) nm CeO_2 nanoflowers were formed at $R_{OA:OM}$ = 1:3 (Figure 1b). Further increasing $R_{OA/OM}$ to 2:3 resulted in star-shaped nanoflowers with a size of (10.6 ± 1.4) nm and exposed (100) facets (Figure 5c and Table 1). As $R_{OA/OM}$ increased from 1:6 to 1:3, the size of the CeO_2 nanoflowers increased, possibly because the rate of 3D oriented attachment was accelerated by the additional amount of oleic acid. However, as $R_{OA/OM}$ increased from 1:3 to 2:3, the size of CeO_2 nanoflowers decreased remarkably, possibly because the rate of 3D oriented attachment was markedly inhibited by the excess of oleic acid (see Figure S3b,c in the Supporting Information). These results reveal that addition of OA to OM promotes oriented attachment among small ceria nanoparticles and formation of various nanostructures depending on $R_{OA/OM}$.

Amount of precursor: At $R_{OA:OM}$ = 1:3 (300 °C, 1 h), when the amount of precursor n_p was decreased from 1 to 0.5 and then to 0.2 mmol, the size of the CeO_2 nanoflowers decreased from (33.8 ± 2.3) (Figure 1b and Table 1) to (17.8 ± 1.1) (Figure 5d and Table 1) and then to (16.3 ± 2.4) nm (Figure 5e and Table 1), respectively, accompanied by transformation from cube- to star-shaped nanoflowers (Figures 1b and 5d,e). We suggest that the shape of the CeO_2 nanoflowers is decided by the ratio of n_p and $R_{OA/OM}$. When the ratio of n_p and $R_{OA/OM}$ increased, transformation of the 3D structure from cube- to star-shaped occurred.

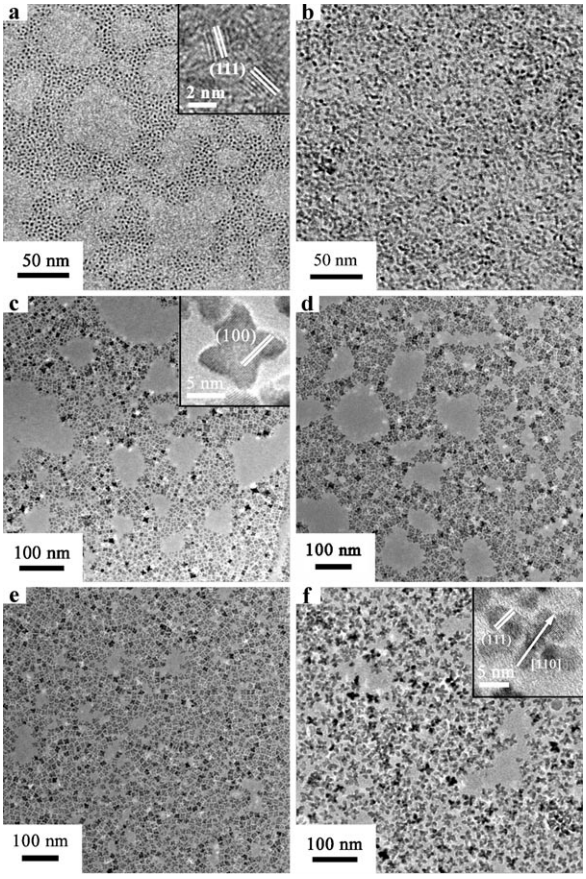

Figure 5. TEM images of CeO_2 nanocrystals synthesized under different conditions: a) 1 mmol of $(NH_4)_2Ce(NO_3)_6$, OA:OM = 0:1, 300 °C, 1 h; b) 1 mmol of $(NH_4)_2Ce(NO_3)_6$, OA:OM = 1:6, 300 °C, 1 h; c) 1 mmol of $(NH_4)_2Ce(NO_3)_6$, OA:OM = 2:3, 300 °C, 1 h; d) 0.5 mmol of $(NH_4)_2Ce(NO_3)_6$, OA:OM = 1:3, 300 °C, 1 h; e) 0.2 mmol of $(NH_4)_2Ce(NO_3)_6$, OA:OM = 1:3, 300 °C, 1 h; f) 1 mmol of $(NH_4)_2Ce(NO_3)_6$, OA:OM = 1:3, 230 °C, 30 min.

Reaction time and temperature: The shape and size of the CeO_2 nanoflowers can also be tuned by changing the reaction temperature and reaction time. For instance, with 1 mmol of $(NH_4)_2Ce(NO_3)_6$ as precursor, reaction at 230 °C

for 0.5 h with OA:OM = 1:3 yielded four-petaled nanoflowers with a size of (28.5 ± 1.9) nm (Figure 5 f and Table 1). The HRTEM image inset in Figure 5 f shows that the four-petaled nanoflowers are composed of building blocks joined along (110) and (111) planes. This implies that 3D oriented attachment would be restricted at low temperatures. On increasing the reaction time from 1 to 4 h at 300 °C, the size of the nanoflowers increased from 33.8 to 37.6 nm (Figure 1 b,e and Table 1).

Formation mechanism of CeO_2 nanoflowers: We attempted to elucidate the formation mechanism of CeO_2 nanoflowers in carefully designed and condition-dependent experiments. In addition to TEM and UV/Vis measurements, for the first time, an in situ electrical conductance technique was introduced into the reaction medium in order to track the growth stages of the nanoflowers.

Monitoring the formation of CeO_2 nanoflowers by in situ electrical conductance measurements: The in situ UV/Vis technique has been successfully developed to study the growth kinetics of high-quality colloidal inorganic nanocrystals including oxides (e.g., Fe_3O_4) and semiconductors (e.g., CdSe) due to their unique size/shape-dependent optical properties.[5] In this work, an in situ electrical conductivity technique was used to probe the growth kinetics of CeO_2 nanoflowers. We used a multimeter (0–200 MΩ) to monitor the electrical conductance of the reaction solution, with two Pt electrodes directly immersed in the solution. The solutions were classified as follows: highly conductive for resistance $R < 10$ MΩ, and nonconductive for $R > 200$ MΩ.

First, the conductance of several solutions was measured in order to verify the presence of conductive ions in this reaction system. We found that OM and OA were nonconductive, and the solvent mixture (10 mmol of OA and 30 mmol of OM) was nonconductive at 140 °C but weakly conductive at 300 °C ($R \approx 50$ MΩ). When $(NH_4)_2Ce(NO_3)_6$ dissolved in OM, the solution was still nonconductive, that is, $(NH_4)_2Ce(NO_3)_6$ is apparently dispersed in OM but not ionized. However, when $(NH_4)_2Ce(NO_3)_6$ was dissolved in OA:OM (1:3), the solution became conductive ($R \approx 3.2$ MΩ), that is, $(NH_4)_2Ce(NO_3)_6$ was ionized in this case. To further identify the conductive ions in the reaction solutions, $Ce(OH)_4$, $Ce(NO_3)_3{\cdot}6H_2O$, and NH_4NO_3 were mixed with OA or OM at 140 °C with vigorous magnetic stirring under vacuum for 30 min (to remove water), respectively. We found that both $Ce(OH)_4$ and $Ce(NO_3)_3{\cdot}6H_2O$ could not dissolve in OM, and NH_4NO_3 could not dissolve in OA. NH_4NO_3 could dissolve in OM but showed no conductance. $Ce(OH)_4$ and $Ce(NO_3)_3{\cdot}6H_2O$ could dissolve in OA, and the solution showed weak conductance at 300 °C in the case of the former ($R \approx 50$ MΩ), but strong conductance at room temperature for the latter ($R \approx 1.4$ MΩ). Further experiments showed that $Ce(OH)_4$ and $Ce(NO_3)_3{\cdot}6H_2O$ can form $[Ce(OA)_{4-x}]^{x+}$ in OA after a long period of standing at 140 °C under vacuum (see Figure S4 in the Supporting Information); therefore, we suggested that $[Ce(OA)_{4-x}]^{x+}$ is weakly conductive, while NO_3^- ions are strongly conductive. Finally, we deduced that the in situ electrical conductance technique might be used to monitor the consumption of NO_3^- ions in $(NH_4)_2Ce(NO_3)_6$/OA/OM, and even the consumption of the monomers with temperature and time during the formation of CeO_2 nanoflowers (see Figure 6 a and Figure S5 in the Supporting Information). In the following, we describe the growth kinetics of CeO_2 nanoflowers, based on the combined results obtained by means of the in situ electrical conductance technique, TEM measurements, and UV/Vis spectroscopy.

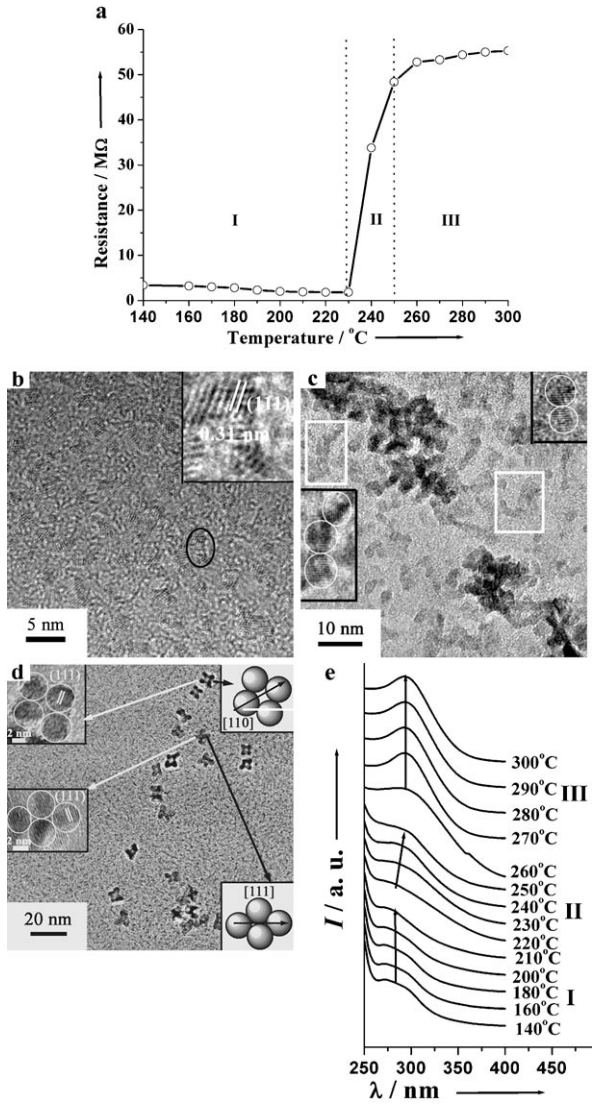

Figure 6. a) Electrical resistance as a function of temperature in the synthesis of 33.8 nm CeO_2 nanoflowers (1 mmol of $(NH_4)_2Ce(NO_3)_6$, OA:OM = 1:3, 0 min). TEM and HRTEM images (inset) of CeO_2 nanocrystals obtained at b) 140, c) 230, and d) 240 °C (inset, left: HRTEM images of solid (top) and hollow (bottom) attachment; right: model patterns of the corresponding HRTEM images) with 1 mmol of $(NH_4)_2Ce(NO_3)_6$ as precursor, OA:OM = 1:3, 0 min. e) Dependence of UV/Vis absorption on temperature for the synthesis of 33.8 nm CeO_2 nanoflowers (1 mmol of $(NH_4)_2Ce(NO_3)_6$, OA:OM = 1:3, 0 min).

Nucleation (stage I): generation of primary ceria cluster particles: Figure 6a shows a typical plot of *R* versus temperature during the synthesis of 33.8 nm CeO_2 nanoflowers. As the temperature rose from 140 to 220 °C, *R* decreased gradually from 3.4 to 1.8 MΩ (Stage I), that is, OA molecules replaced more NO_3^- anions to bond with ceria clusters, and hence more NO_3^- ions were released at elevated temperature within this range. As shown in Figure 6b, ceria clusters (either discrete or aggregated from two or three 2 nm truncated octahedron-like particles) were formed in this temperature range. The HRTEM image inset in Figure 6b reveals that these clusters mainly exposed (111) planes, which is the most stable plane for face-centered cubic materials in theory.[9] Since $(NH_4)_2Ce(NO_3)_6$ can not dissolve in OA, the ceria clusters should not be derived from the $[Ce(OA)_{4-x}]^{x+}$ species (see FTIR results in Figure S4 in the Supporting Information). To account for the in situ electrical conductance data and TEM results together, we suggest that formation of ceria clusters did not consume the free NO_3^- ions. In fact, $(NH_4)_2Ce(NO_3)_6$ was found to decompose at about 220 °C by thermogravimetric/differential thermal analysis (TG/DTA, see Figure S6 in the Supporting Information). In addition, GC-MS characterization was utilized to investigate the decomposition kinetics of $(NH_4)_2Ce(NO_3)_6$. No ion fragments were detectable at about 140 °C, that is, thermolysis with bond cleavage of the precursor did not take place in stage I. Therefore, formation of the ceria clusters should not result from decomposition of $(NH_4)_2Ce(NO_3)_6$ at temperatures below 220 °C. In conclusion, we suggest that the ceria clusters were formed via the hydrolysis of $(NH_4)_2Ce(NO_3)_6$ in the presence of some extra water in the solution (see Figure S7 in the Supporting Information).

Now we can describe the nucleation stage in the following way: Initially, $(NH_4)_2Ce(NO_3)_6$ dissolved in OM, NO_3^- ions were gradually substituted by OA, and detectable conductance resulted from the free NO_3^- ions in solution. Simultaneously, the monomers were hydrolyzed and the ceria clusters were thus formed, while NO_3^- ions and surfactant ligands (OA and OM) were strongly adsorbed on the surface of the ceria clusters.

Crystal growth (stages II & III): secondary self-organization into CeO_2 nanoflowers by 3D oriented attachment: The evolution of the CeO_2 nanoflowers by oriented attachment is shown in Figure 6b–d.The building blocks of the nanoflowers are 2 nm CeO_2 truncated octahedron-like particles formed in the nucleation stage of the reaction (from 140 to 220 °C, see Figure 6b). However, on increasing the temperature to 230 °C, CeO_2 clusters were formed by oriented attachment of two or three of these particles, with the direction of attachment along (111) planes (Figure 6c).[13] When the temperature increased further (>240 °C), 2D nanostructures containing four building blocks were obtained by solid or hollow attachment. Careful analysis of the HRTEM images and the models of these 2D nanostructures (Figure 6d, insets) showed that the extended direction was along [111] for the solid structure, and along [110] for the hollow structure, while oriented attachment of both proceeded along (111) planes. When the temperature exceeded 250 °C (Figure 7a), cube-shaped nanoflowers were formed, mainly with exposed {100} planes.

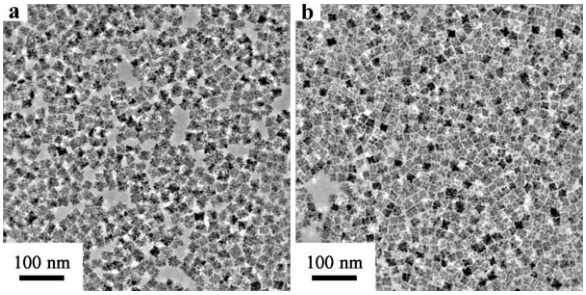

Figure 7. TEM images of CeO_2 nanoflowers obtained at a) 250 °C for 0 min and b) 300 °C for 10 h (1 mmol of $(NH_4)_2Ce(NO_3)_6$, OA:OM = 1:3).

As shown in the conductance plot (Figure 6a), in stage II between 230 and 250 °C, a sudden rise in resistance from 1.8 to 48.4 MΩ was observed, that is, the NO_3^- ions were exhausted at this stage. From the TEM images, 2D nanostructures of ceria formed by either solid or hollow attachment, together with some truncated octahedron-like particles, could be found at temperatures from 230 (Figure 6b) to 240 °C (Figure 6c), while only cube-shaped ceria nanoflowers were seen at 250 °C (Figure 7a). All these results strongly suggest that 3D oriented attachment took place in this stage, mainly because the sudden loss of the adsorbed NO_3^- ions on decomposition exposed some active facets with high surface energy. Moreover, the 3D oriented attachment showed a favored direction of [111], presumably because the preferred adsorption of surfactant ligands (mainly OA molecules) on some specific facets (e.g., {100} rather than {111}) considerably reduced the energy of these facets and made them less accessible during the attachment process.

To further confirm the above speculation, interactions between NO_3^- ions and the ceria clusters were investigated by using $Ce(OH)_4$ and NH_4NO_3 as precursors for the synthesis of CeO_2 nanocrystals. Although NO_3^- ions were dissociated in this case (see Figure S8), no CeO_2 nanoflowers were obtained (see Figure S9 in the Supporting Information), indicative of less adsorption of NO_3^- ions onto the surfaces of the ceria seeds formed from $Ce(OH)_4$. Consequently, with $(NH_4)_2Ce(NO_3)_6$ as precursor, the formation of the nanoflowers should be mainly due to strong adhesion of dissociated NO_3^- ions from $(NH_4)_2Ce(NO_3)_6$ to the surfaces of the ceria clusters. Furthermore, there may be some complicated interactions among the adsorbed species (such as NO_3^- and $[Ce(NO_3)_{6-x}]^{x-2}$ ions) and surrounding species (such as OM and NH_4^+, which contacted with NO_3^- and $[Ce(NO_3)_{6-x}]^{x-2}$ ions) for the ceria clusters, as $(NH_4)_2Ce(NO_3)_6$ was dissolved in OM. In the second stage, the strong redox reaction intrinsic to $(NH_4)_2Ce(NO_3)_6$ (see TG/DTA results in Figure S7 in the Supporting Information) and between this strong oxidizing agent and the reducing surfactant ligands incorporated

with C=C bonds (see GC-MS results in Figure S10 in the Supporting Information) occurred.[14] At this moment, the ligand surface coverage of the ceria clusters was significantly reduced due to removal of the NO_3^- and OM ligands but not OA coating the ceria clusters (see Figure S11 in the Supporting Information), and 3D oriented attachment occurred. Our further experiments confirmed that the (111) facets of the ceria nanocrystals were not as stable as the (100) facets when OA was in excess (see Figure S12 in the Supporting Information). We found that OA molecules can stabilize the (100) facets by coordinative interaction. When the temperature increased, the (100) facets became the most stable due to the strong bonding of OA ligands. This result indicates that OA might be preferably adsorbed onto the {100} facets. In conclusion, not only because of insufficient ligands on particular facets (mainly (111) facets) of the ceria clusters caused by decomposition of $(NH_4)_2Ce(NO_3)_6$, but also due to the preferred adsorption of OA on {100} facets, the ceria clusters were likely to self-assemble into nanoflowers mainly exposing {100} planes by 3D oriented attachment along [111] planes in stage II, in order to minimize the total surface energy of the whole particle system.

Beyond 250 °C (Stage III), the variation of the solution resistance was moderate (Figure 6a), that is, the NO_3^- ions were consumed completely. Under these conditions, uniform ceria nanoflowers were formed. Moreover, their morphologies remained stable (see Figure 7b) even when heated at 300 °C for 10 h, which indicates that the total surface energy of the nanoflowers is quite low. With increasing reaction temperature and time, only the size of the nanoflowers slightly increased (Figure 7a: 28.4 nm at 250 °C for 0 min; Figure 1b: 33.8 nm at 300 °C for 1 h). As a result, we suggest that, in this stage, Ostwald ripening occurred as the monomers were used up (as revealed by exhaustion of the NO_3^- ions in the conductance plot shown in Figure 6a).

The UV/Vis absorption (Figure 6e) is consistent with the conductance analysis and TEM characterization. In the first stage, the UV absorption edge was steady due to the absorption of both the truncated octahedron-like ceria particles unaltered in size and the monomers, while during the second stage a red shift in UV absorption edge was apparent due to 3D oriented attachment of the CeO_2 clusters to the nanoflowers and gradual consumption of the monomers (see also Figure 3b and Figure S13 in the Supporting Information). In the third stage, the UV/Vis absorption edges of the samples taken at various temperatures were similar, which also implies that the shape of the CeO_2 nanoflowers was likely invariant under conditions where the monomers were consumed completely.

A suggested scheme for the formation of ceria nanoflowers: A possible formation mechanism of the CeO_2 nanoflowers is shown in Scheme 1. At the very beginning, some ceria clusters (discrete truncated octahedron-like particles and aggregates containing two or three such particles) are formed by hydrolysis of $(NH_4)_2Ce(NO_3)_6$ in the OA:OM mixed solvent at temperatures from 140 to 220 °C. Simultaneously, abundant ligands (e.g., OA, OM, and NO_3^-) are adsorbed on the cluster surfaces, among which the {100} facets interact strongly with OA molecules. Then, the strong redox reaction intrinsic to $(NH_4)_2Ce(NO_3)_6$ and between this strong oxidizing agent and the reducing surfactant ligands incorporated with C=C bonds took place suddenly at a temperature close to 220 °C. In this moment, the adsorbed ligands (mainly NO_3^- and the surrounding OM^+) on the surfaces of CeO_2 clusters vanish dramatically. As a result, to reduce the total energy of the whole particle system, CeO_2 nanoflowers with exposed (100) facets are spontaneously formed from the small CeO_2 clusters by 3D oriented attachment at temperatures above 220 °C, with coalescence of the active (111) facets due to insufficient ligand protection.[13] In contrast to the work of Peng et al.,[1k,l] our 3D oriented attachment is a spontaneous process, for which the strong redox reaction is essential.

When $Ce(NO_3)_3{\cdot}6H_2O$ or $Ce(OH)_4$ was used as precursor, no rapid strong redox reaction occurred. As the temperature

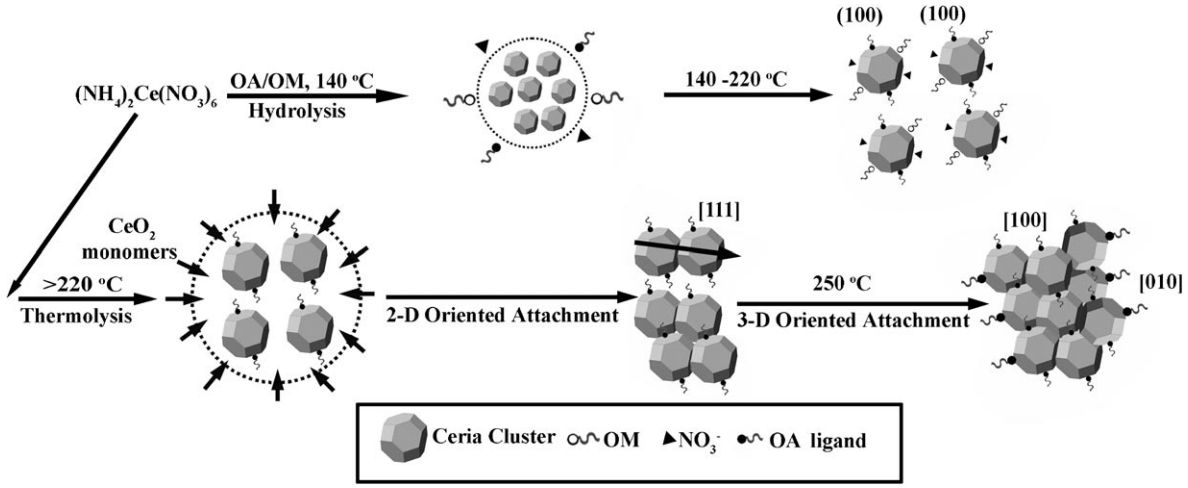

Scheme 1. Schematic illustration of the growth stages of CeO_2 nanoflowers.

increased, the ligands on the surface of the particles decomposed gradually (different from the case of $(NH_4)_2Ce(NO_3)_6$, which is a very strong oxidizing agent ($E° \approx 0.96$ V vs. NHE).[14] Because not enough active surfaces were exposed simultaneously when the ligands were gradually removed, only Ostwald ripening but not 3D oriented attachment occurred. As a result, ceria nanopolyhedra with random aggregation were formed (see Figure 4a), no matter whether NH_4NO_3 was added in the synthesis. Our further experiments showed that the strong coordination between Ce^{4+} ions and the $RCOO^-$ ligands makes it difficult to remove the coordinated $RCOO^-$ ligands abruptly by adding another reagent (see Figure S14 in the Supporting Information). Therefore, abrupt loss of the surface ligands for the ceria clusters is the key to the formation of the CeO_2 nanoflowers. In summary, insufficient surface ligand coverage on particular facets ({111}) of ceria clusters, produced by the strong redox reaction of $(NH_4)_2Ce(NO_3)_6$ in OA/OM, provides the required driving force for kinetic formation of the present CeO_2 nanoflowers by 3D oriented attachment.

Above 220 °C, uniform ceria nanoflowers were formed from the preformed ceria cluster seeds with continuous consumption of the ceria monomers (released by decomposition of the $(NH_4)_2Ce(NO_3)_6$ precursor at 220 °C in the above strong redox reaction) as 3D oriented attachment continued, due to a well-maintained balance of the nucleation and growth stages.[1,3]

Catalytic activity of CeO_2 nanoflowers in CO oxidation: Oxidation of CO was selected to test the catalytic activity of the as-obtained 33.8 nm CeO_2 nanoflowers. For comparison, (11.5 ± 1.8) nm CeO_2 nanopolyhedra (enclosed by six (100) and eight (111) facets) and (36.1 ± 7.1) nm CeO_2 nanocubes (enclosed by six (100) facets) were prepared by a hydrothermal method we developed before.[6c] The catalysts were obtained by calcination at 400 °C for 4 h in still air. Perhaps due to the 3D structure of the nanoflowers, together with the violent removal of the capping ligands by calcination, the as-calcined nanoflowers are highly porous in nature (see Figure S15 in the Supporting Information) and have a quite large BET specific surface area of 156 $m^2 g^{-1}$. This value is nearly 1.7 times that of 91 $m^2 g^{-1}$ for the as-calcined nanopolyhedra, and 4.7 times that of 33 $m^2 g^{-1}$ for the as-calcined nanocubes.

Figure 8 shows a plot of CO conversion versus reaction temperature for the as-prepared CeO_2 catalysts. For CO conversion to CO_2 from 200 to 400 °C, the activity of the catalysts followed the trend of nanoflowers > nanopolyhedra > nanocubes, in good agreement with the order of the specific surface areas. This result indicates that the catalyst with higher specific surface area could provide more active sites for CO conversion. Furthermore, the temperature for 50% CO conversion of the as-calcined nanoflowers is as low as 250 °C, where the CO conversion is 29% for the nanopolyhedra, and 15% for the nanocubes. Furthermore, even at 400 °C, these two catalysts had still not attained 100% CO conversion. The CO conversion at 400 °C is 81% for the nanopolyhedra, and only 33% for the nanocubes.

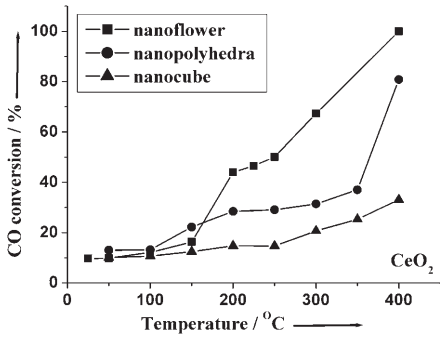

Figure 8. CO conversion versus reaction temperature over ceria nanopolyhedron, nanocube, and nanoflower catalysts.

Conclusion

On the basis of a unique 3D oriented-attachment mechanism, uniform CeO_2 nanoflowers with controlled shape (cubic, four-petaled, and starlike) and size (10–40 nm) were synthesized in hot oleic acid (OA)/oleylamine (OM) solutions by using $(NH_4)_2Ce(NO_3)_6$ as precursor. Shape and size control were realized by changing the solvent composition (OA:OM ratio), precursor concentration, and reaction temperature and time. The whole formation process of the nanoflowers was monitored by an in situ electrical conductance technique, with assistance from TEM measurements and UV/Vis spectroscopy. The nanoflowers were found to be formed in two main steps: 1) formation of CeO_2 primary cluster particles via hydrolysis of $(NH_4)_2Ce(NO_3)_6$ above 140 °C, the surfaces of which adsorb abundant ligands including OA, OM, and NO_3^-, and 2) secondary self-assembly of the primary particles into nanoflowers above 220 °C due to the significant reduction in surface ligand coverage caused by the abrupt decomposition of $(NH_4)_2Ce(NO_3)_6$ at the elevated temperature in a strong redox reaction. Furthermore, extension of this reaction mechanism to the synthesis of CoO, NiO, and CuO_x nanoflowers with interesting magnetic properties (Table 1 and Figures S16–S18 in the Supporting Information) demonstrates the versatility of the present synthetic approach. The as-calcined 33.8 nm CeO_2 nanoflowers are very active for CO conversion to CO_2 at low temperatures in the range 200–400 °C owing to the high specific surface area (156 $m^2 g^{-1}$) of the porous 3D structure. This work represents an important step forward in the construction of more complex 3D nanostructures of colloidal inorganic nanocrystals with useful material properties, and has opened up the possibility of using the in situ electrical conductance method to reveal the principles of nanocrystal growth kinetics in solutions.

Experimental Section

Chemicals: Ceric ammonium nitrate ($(NH_4)_2Ce(NO_3)_6$, Sigma-Aldrich), oleic acid (OA; 90%, Alpha), oleylamine (OM; >80%, Acros), $Ce(NO_3)_3{\cdot}6H_2O$ (Beijing Chem. Corp. China), NH_4NO_3 (Beijing Chem. Corp. China), aqueous ammonia, absolute ethanol, and hexane were used as received without further purification. $(NH_4)_3M(NO_3)_5$ (M = Co, Ni, Cu) were obtained by the preparation method described in the literature.[15] $Ce(OH)_4$ was prepared by the precipitation reaction between $(NH_4)_2Ce(NO_3)_6$ and ammonia in H_2O.

Nanoflower synthesis: All nanocrystals were synthesized by using standard oxygen-free procedures. **Caution!** Although not encountered in our experiments, $(NH_4)_2Ce(NO_3)_6$ is potentially explosive. Only a small amount of the material should be prepared, and it should be handled with care.

Synthesis of CeO_2 nanoflowers: **Caution!** Use appropriate safety measures to avoid the overpressure caused by the fierce decomposition of $(NH_4)_2Ce(NO_3)_6$ as the temperature approaches 220 °C.

Typical procedure: 1 mmol of $(NH_4)_2Ce(NO_3)_6$, 10 mmol of oleic acid, and 30 mmol of oleylamine were added to a three-necked round-bottom flask (100 mL) containing a spin bar. The flask was heated to 140 °C with vigorous magnetic stirring, and kept for 30 min at this temperature under a vacuum to remove water and oxygen, resulting in the formation of a clear light yellow solution. Then, the stock solution was heated to a given temperature in the range 230–300 °C at a rate of approximately 12 °C min^{-1} under an Ar atmosphere, and kept at this temperature for 30–60 min. On heating near 220 °C, the reaction solution suddenly became turbid, with the release of a huge amount of gas bubbles. Meanwhile, its color turned to brown, which suggested the beginning of CeO_2 nanoflower formation. When the reaction was complete, an excess of ethanol was poured into the solution at room temperature. The resultant turbid suspension was centrifugally separated, and the product was collected. The precipitates were washed several times with ethanol and dried in air at 70 °C overnight, and yellow powders of CeO_2 nanoflowers were thus obtained in a yield of around 60–70% (Table 1). They can be easily redispersed in various nonpolar organic solvents (e.g., hexane). The as-prepared CeO_2 nanocrystals were calcined at 400 °C for 4 h in still air for measurements of specific surface area and CO oxidation conversion.

Synthesis of CoO, NiO, and CuO_x nanoflowers: The synthetic procedure was the same as that used to synthesize CeO_2 nanoflowers, except that $(NH_4)_3M(NO_3)_5$ (M = Co, Ni, Cu)[15] were used as precursors (Table 1).

Characterization: Powder XRD patterns of the dried powders were recorded on a Rigaku D/MAX-2000 diffractometer (Japan) with a slit of 1/2° at a scanning rate of 2 min^{-1} with $Cu_{K\alpha}$ radiation ($\lambda = 1.5406$ Å). The lattice parameters were calculated with the least-squares method. The average crystal domain size of the nanoflowers grain size D was estimated with Scherrer equation [Eq. (1)]

$$D = \frac{0.9\lambda}{\beta \cos\theta} \quad (1)$$

where θ is the diffraction angle of the (111) peak of the cubic phase and β the full width at half-maximum of the (111) peak in radians, calibrated with high-purity silicon. Samples for transmission electron microscopy (TEM) analysis were prepared by drying a nanocrystal dispersion in hexane on amorphous carbon-coated copper grids. Particle sizes and shapes were examined by TEM (200CX, JEOL, Japan) at 160 kV. High-resolution TEM (HRTEM) characterization was performed with a Philips Tecnai F30 FEG-TEM operated at 300 kV. The electrical resistance of the solution was measured by a multimeter (Model MY63: 0–200 MΩ, Shenzhen Huayi Mastech), with two Pt electrodes immersed in the solution. The BET specific surface area S_{BET} was measured by nitrogen adsorption at 78.3 K on an ASAP 2010 analyzer (Micromeritics Co. Ltd.), and measurements were performed after outgassing the sample at 423 K for 4 h under vacuum, down to a residual pressure better than 10^{-3} Torr.

The combined TG-DTA runs were performed with a Universal V2.60 TA instrument at a heating rate of 5 °C min^{-1} from room temperature to 600 °C with α-Al_2O_3 as reference. FTIR spectra were obtained on a Nicolet Magna 750 FTIR spectrometer at a resolution of 4 cm^{-1} with a Nic-Plan IR microscope. The UV/Vis spectra of the nanocrystal dispersions were recorded on a HITACHI U-3010 spectrometer in a quartz cell (1 cm path length), and pure hexane was used as blank. The optical absorption coefficient α was calculated according to Equation (2)[11f]

$$\alpha = (2.303 \times 10^3 Ap)/lc \quad (2)$$

where A is the absorbance of the sample, ρ the real density of CeO_2 (7.28 g cm^{-3}), l the path length, and c the concentration of the ceria suspension.

CO oxidization test: A home-made flow reactor system including a quartz reaction tube (8×42 mm) was used for the catalytic test. In a typical CO oxidation experiment, 50 mg of as-calcined CeO_2 nanocrystals and 450 mg of sea sand were mixed as catalyst, and the experiment was carried out under a flow of reactant gas mixture (0.5% CO, 10% O_2, balance N_2) at a rate of 50 mL min^{-1}. The composition of the gas was monitored on-line by gas chromatography (Shimadzu, GC-14C).

Magnetic measurements: The magnetic measurements were performed on a MPMS-XL-5 superconductive quantum interference device (SQUID) magnetometer (Quantum Design, USA). The curve of magnetization versus absolute temperature for the CoO nanocrystals was recorded under an applied field of 1000 Oe.

Acknowledgement

We gratefully acknowledge financial aid from the MOST of China (Grant No. 2006CB601104), the NSFC (Grant Nos. 20571003, 20221101, and 20423005), and the MOE of China (Grant No. 20060001027).

[1] a) C. B. Murray, D. J. Norris, M. G. Bawendi, *J. Am. Chem. Soc.* **1993**, *115*, 8706; b) A. P. Alivisatos, *Science* **1996**, *271*, 933; c) S. Sun, C. B. Murray, D. Weller, L. Folks, A. Moser, *Science* **2000**, *287*, 1989; d) J. Park, K. An, Y. Hwang, J. G. Park, H. J. Noh, J. Y. Kim, J. H. Park, N. M. Hwang, T. Hyeon, *Nat. Mater.* **2004**, *3*, 891; e) X. G. Peng, L. Manna, W. D. Yang, J. Wickham, E. Scher, A. Kadavanich, A. P. Alivisatos, *Nature* **2000**, *404*, 59; f) M. B. Sigman, A. Ghezelbash, T. Hanrath, A. E. Saunders, F. Lee, B. A. Korgel, *J. Am. Chem. Soc.* **2003**, *125*, 16050; g) B. D. Yuhas, D. O. Zitoun, P. J. Pauzauskie, R. He, P. Yang, *Angew. Chem.* **2006**, *118*, 434; *Angew. Chem. Int. Ed.* **2006**, *45*, 420; h) X. Sun, Y. W. Zhang, Y. P. Du, Z. G. Yan, R. Si, L. P. You, C. H. Yan, *Chem. Eur. J.* **2007**, *13*, 2320; i) R. Si, Y. W. Zhang, H. P. Zhou, L. D. Sun, C. H. Yan, *Chem. Mater.* **2007**, *19*, 18; j) V. F. Puntes, D. Zanchet, C. K. Erdonmez, A. P. Alivisatos, *J. Am. Chem. Soc.* **2002**, *124*, 12874; k) A. Narayanaswamy, H. F. Xu, N. Pradhan, X. G. Peng, *Angew. Chem.* **2006**, *118*, 5487; *Angew. Chem. Int. Ed.* **2006**, *45*, 5361; l) A. Narayanaswamy, H. F. Xu, N. Pradhan, M. Kim, X. G. Peng, *J. Am. Chem. Soc.* **2006**, *128*, 10310.

[2] a) L. Manna, E. C. Scher, A. P. Alivisatos, *J. Am. Chem. Soc.* **2000**, *122*, 12700; b) S. I. Cha, C. B. Mo, K. T. Kim, S. H. Hong, *J. Mater. Res.* **2005**, *20*, 2148; c) B. K. Jena, C. R. Raj, *Langmuir* **2007**, *23*, 4064; d) T. Wang, X. Hu, S. Dong, *J. Phys. Chem. B* **2006**, *110*, 16930; e) X. Teng, S. Maksimuk, S. Frommer, H. Yang, *Chem. Mater.* **2007**, *19*, 36.

[3] a) Y. D. Yin, A. P. Alivisatos, *Nature* **2005**, *437*, 664; b) Y. W. Jun, J. H. Lee, J. S. Choi, J. Cheon, *J. Phys. Chem. B* **2005**, *109*, 14795; c) T. Hyeon, *Chem. Commun.* **2003**, 927; d) W. C. W. Chan, S. Nie, *Science* **1998**, *281*, 2016; e) Y. W. Jun, J. S. Choi, J. W. Cheon, *Angew. Chem.* **2006**, *118*, 3492; *Angew. Chem. Int. Ed.* **2006**, *45*, 3414.

[4] a) I. Gur, N. A. Fromer, M. L. Geier, A. P. Alivisatos, *Science* **2005**, *310*, 462; b) M. Law, D. J. Sirbuly, J. C. Johnson, J. Goldberger, R. J. Saykally, P. D. Yang, *Science* **2004**, *305*, 1269; c) N. Pinna, G. Neri, M. Antonietti, M. Niederberger, *Angew. Chem.* **2004**, *116*, 4445; *Angew. Chem. Int. Ed.* **2004**, *43*, 4345; d) M. Bruchez, M. Moronne, P. Gin, S. Weiss, A. P. Alivisatos, *Science* **1998**, *281*, 2013.

[5] a) M. F. Casula, Y. W. Jun, D. J. Zaziski, E. M. Chan, A. Corrias, A. P. Alivisatos, *J. Am. Chem. Soc.* **2006**, *128*, 1675; b) Z. A. Peng, X. G. Peng, *J. Am. Chem. Soc.* **2002**, *124*, 3343.

[6] a) Q. Fu, H. Saltsburg, M. Flytzani-Stephanopoulos, *Science* **2003**, *301*, 935; b) K. B. Zhou, X. Wang, X. M. Sun, Q. Peng, Y. D. Li, *J. Catal.* **2005**, *229*, 206; c) H. X. Mai, L. D. Sun, Y. W. Zhang, R. Si, W. Feng, H. P. Zhang, H. C. Liu, C. H. Yan, *J. Phys. Chem. B* **2005**, *109*, 24380; d) J. Kašpar, P. Fornasiero, M. Graziani, *Catal. Today* **1999**, *50*, 285; e) E. P. Murray, T. Tsai, S. A. Barnett, *Nature* **1999**, *400*, 649; f) A. Corma, P. Atienzar, H. Garcia, J. Y. Chane-Ching, *Nat. Mater.* **2004**, *3*, 394; g) L. Tye, N. A. El-Masry, T. Chikyowm, P. McLarty, S. M. Bedair, *Appl. Phys. Lett.* **1994**, *65*, 3081; h) A. H. Morshed, M. E. Moussa, S. M. Bedair, R. Leonard, S. X. Liu, N. El-Masry, *Appl. Phys. Lett.* **1997**, *70*, 1647.

[7] a) C. Kittel, *Introduction to Solid State Physics, Vol. 1*, 6th ed., Wiley, New York, **1986**; b) F. A. Cotton, G. Wilkinson, M. Bochmann, C. Murillo, *Advanced Inorganic Chemistry*, 6th ed., Wiley, New York, **1999**; c) R. Weissleder, *Radiology* **1999**, *212*, 609; d) O. Giraldo, S. L. Brock, W. S. Willis, M. Marquez, S. L. Suib, S. Ching, *J. Am. Chem. Soc.* **2000**, *122*, 9330; e) J. M. Tarascon, M. Armand, *Nature* **2001**, *414*, 359; f) F. Patolsky, Y. Weizmann, E. Katz, I. Willner, *Angew. Chem.* **2003**, *115*, 2474, *Angew. Chem. Int. Ed.* **2003**, *42*, 2372.

[8] L. Qian, X. R. Yang, *J. Phys. Chem. B* **2006**, *110*, 16672.

[9] a) T. X. T. Sayle, S. C. Parker, C. R. A. Catlow, *Surf. Sci.* **1994**, *316*, 329; b) J. C. Conesa, *Surf. Sci.* **1995**, *339*, 337; c) D. C. Sayle, S. A. Maicaneanu, G. W. Watson, *J. Am. Chem. Soc.* **2002**, *124*, 11429.

[10] F. L. Normand, L. Hilaire, K. Kili, G. Krill, G. Maire, *J. Phys. Chem.* **1988**, *92*, 2561.

[11] a) I. Kosacki, V. Petrovsky, H. U. Anderson, P. Colomban, *J. Am. Ceram. Soc.* **2002**, *85*, 2646; b) W. H. Weber, K. C. Hass, J. R. McBride, *Phys. Rev. B* **1993**, *48*, 178; c) I. Kosacki, T. Suzuki, H. U. Anderson, P. Colomban, *Solid State Ionics* **2002**, *149*, 99.

[12] a) F. Marabelli, P. Wachter, *Phys. Rev. B* **1987**, **36**, 1238; b) V. Petrovsky, B. P. Gorman, H. U. Anderson, T. Petrovsky, *J. Appl. Phys.* **2001**, *90*, 2517; c) M. D. Hernandez-Alonso, A. B. Hungria, A. Martinez-Arias, J. M. Coronado, *Phys. Chem. Chem. Phys.* **2004**, *6*, 3524; d) S. Tsunekawa, T. Fukuda, A. Kasuya, *J. Appl. Phys.* **2000**, *87*, 1318; e) P. Patsalas, S. Logothetidis, *Phys. Rev. B* **2003**, *68*, 035104; f) Y. W. Zhang, R. Si, C. S. Liao, C. H. Yan, C. X. Xiao, Y. Kou, *J. Phys. Chem.* B **2003**, *107*, 10159.

[13] R. L. Penn, J. F. Banfield, *Science* **1998**, *281*, 969.

[14] V. Nair, A. Deepthi, *Chem. Rev.* **2007**, *107*, 1862.

[15] I. V. Morozov, A. A. Fedorova, S. I. Troyanov, *Z. Anorg. Allg. Chem.* **1998**, *624*, 1543.

Received: August 28, 2007
Revised: November 28, 2007
Published online: February 7, 2008

